Applied Catalysis B: Environmental 134–135 (2013) 293–301

Contents lists available at SciVerse ScienceDirect

Applied Catalysis B: Environmental

journal homepage: www.elsevier.com/locate/apcatb

Preparation of p–n junction $Cu_2O/BiVO_4$ heterogeneous nanostructures with enhanced visible-light photocatalytic activity

Wenzhong Wang*, Xiangwei Huang, Shuang Wu, Yixi Zhou, Lijuan Wang, Honglong Shi, Yujie Liang, Bin Zou

School of Science, Minzu University of China, Beijing 100081, China

ARTICLE INFO

Article history:
Received 10 August 2012
Received in revised form 5 January 2013
Accepted 14 January 2013
Available online 22 January 2013

Keywords:
p–n junction
Degradation
Photocatalysis
Preparation
$Cu_2O/BiVO_4$ heterogeneous nanostructures

ABSTRACT

p–n junction $Cu_2O/BiVO_4$ heterogeneous nanostructures for enhancement of visible-light photocatalytic properties of $BiVO_4$ nanocrystals have been successfully prepared through coupling a hydrothermal process with polyol strategy. The assembly of p-type Cu_2O nanoparticles produces a large number of nano p–n junction heterostructures on the surface of the $BiVO_4$ nanocrystals, where Cu_2O and $BiVO_4$ form p- and n-type semiconductors, respectively. The experimental results reveal that these p–n junction $Cu_2O/BiVO_4$ heterogeneous nanostructures exhibit much higher visible-light photocatalytic activities than the individual $BiVO_4$ nanocrystals for the degradation of model dyes methylene blue and colorless organic phenol under visible light irradiation. The enhanced photocatalytic efficiencies are attributed to the charge transfer from n-type $BiVO_4$ to the attached p-type Cu_2O nanoparticles, which effectively reduces the recombination of electrons and holes, leading to the enhancement of the photocatalytic properties of the heterostructure nanostructures. These new p–n junction heteronanostructures are expected to show considerable potential applications in solar-driven wastewater treatment.

1. Introduction

The increasing environmental problems have motivated considerable research efforts on photocatalytic pollutant degradation by using visible light that is abundant in the solar spectrum. Therefore many metal oxide semiconductors such as $BiVO_4$ [1,2], Bi_2O_3 [3,4], WO_3 [5,6], Fe_2O [3,7,8] and Cu_2O [9,10] have been developed as photocatalysts with visible-light photocatalytic activities. Among these visible-light photocatalysts, m-$BiVO_4$ with a band gap of ca 2.40 eV [11,12] has been recognized as a potentially suitable visible-light photocatalyst for pollutant decomposition [13–23]. However, it has been reported that the photocatalytic activity of $BiVO_4$ is usually not satisfied because the photogenerated active electrons and holes tend to rapidly decay through recombination [24], which significantly restricted the practical applications of $BiVO_4$ in photocatalytic pollutant degradation. Therefore, it is necessary to develop effective strategies to improve the charge separation efficiency and enhance visible-light photocatalytic activity of $BiVO_4$ photocatalysts.

The previous research work has been demonstrated that combining two or more semiconductors with appropriate band positions can effectively promote their photocatalytic activity because it can considerably improves the electron–hole pairs separation and interfacial charge transfer efficiency [25–29]. For example, $BiVO_4/CeO_2$ nanocomposites [30] and the Bi_2WO_6/TiO_2 hierarchical heterostructure [31] were reported to exhibit much improved photocatalytic performance. Especially, researchers have realized recently that fabrication of a p–n junction in semiconductor photocatalysts is the most effective strategy to significantly promote their photocatalytic performance because of the existence of an internal electric field [32]. For instance, it has been reported that p–n junction Bi_2O_3/Bi_2WO_6 hollow microspheres show an improved photocatalytic performance under visible-light irradiation [33]. In present $Cu_2O/BiVO_4$ composites, Cu_2O is a p-type semiconductor with direct band gap of ca. 2.0 eV and has a noticeable light absorption capability in the visible-light region [34,35]. Accordingly, it is expected to prepare p–n $Cu_2O/BiVO_4$ nanostructures with the highly efficient electron-hole separation and the enhanced photocatalytic activity under visible-light irradiation. Herein we report the preparation of p–n junction $Cu_2O/BiVO_4$ heterogeneous nanostructures by growing Cu_2O nanoparticles on presynthesized $BiVO_4$ nanocrystals through coupling a polyol method with a hydrothermal process. The assembly of p-type Cu_2O nanoparticles produces a large number of nano p–n junction heterostructures on the surface of the $BiVO_4$ nanocrystals. These p–n junction $Cu_2O/BiVO_4$ heterogeneous nanostructures significantly exhibit much higher visible-light photocatalytic activities than the individual $BiVO_4$ nanocrystals for degradation of model dyes methylene blue (MB) and colorless organic phenol. Furthermore, we have discussed the photoinduced electronic interaction

* Corresponding author. Tel.: +86 10 68930239; fax: +86 10 68930239.
E-mail address: wzhwang@aphy.iphy.ac.cn (W. Z. Wang).

0926-3373/$ – see front matter © 2013 Elsevier B.V. All rights reserved.
http://dx.doi.org/10.1016/j.apcatb.2013.01.013

between Cu_2O and $BiVO_4$, in order to have in-depth understanding on the enhanced photocatalytic performance.

2. Experimental

All chemicals used in this work were of analytical reagent grade and used without further purification. Solutions were freshly prepared with deionized water. Bismuth nitrate hexahydrate ($Bi(NO_3)_3{\cdot}5H_2O$), ammonium vanadate (NH_4VO_3), cupric acetate ($Cu(CH_3OO)_2{\cdot}H_2O$), ethylenediaminetetraacetates (EDTA), sodium hydroxide (NaOH), di-ethylene glycol (DEG), nitric acid (HNO_3) and ethanol (EtOH) were purchased from standard sources (China National Medicines Corporation Ltd.)

$BiVO_4$ nanocrystals were synthesized through a hydrothermal process. Briefly, while stirring, 2.42 g of $Bi(NO_3)_3{\cdot}5H_2O$ was initially dissolved in 2 mL of nitric acid, followed by the addition of 7.5 mL of ultrapure water to form a white solution A. Secondly, 0.58 g of NH_4VO_3 was dissolved in 10 mL of 4 M NaOH solution, followed by the addition of 1.00 g of EDTA under stirring to form white solution B. Thirdly, solution B was dropwised into solution A to form a yellow mixture suspension. The pH of the prepared mixture suspension was adjusted to 7 by slowly adding 2 M of NaOH solution. The resultant mixture was then sealed in a 50 mL Teflon-lined stainless-steel autoclave. The autoclave was heated to and maintained at 180 °C for 24 h, and allowed to cool to room temperature. A yellow powder was collected after centrifugation, washed with water repeatedly, and then dried in a vacuum oven.

Cu_2O nanoparticles were grown on the $BiVO_4$ nanocrystals by a polyol method through the following steps. Firstly, 93.45 mg of $Cu(CH_3OO)_2{\cdot}H_2O$ was dissolved in 50 mL of EtOH, followed by the addition of 300 mg of the as-prepared $BiVO_4$ powder to form suspension mixture under sonication to make a quantity ratio of 1:2 of Cu_2O:$BiVO_4$. The mixture was stirred for 6 h and then dried to prepare mixture powder of $Cu(CH_3OO)_2{\cdot}H_2O$ and $BiVO_4$. Secondly, the as-prepared mixture powder of $Cu(CH_3OO)_2{\cdot}H_2O$ and $BiVO_4$ was suspended in 150 mL of DEG solution under sonication, then transferred into a flask with volume of 250 mL. The flask was transferred to an oil bath and heated at 180 °C for 2 h under stirring. The products were separated via centrifugation, washed with water repeatedly, and dried in a vacuum oven.

X-ray powder diffraction (XRD) patterns were recorded on a Rigaku (Japan) Dmax γA rotation anode X-ray diffractometer equipped with graphite monochromatized Cu-Kα radiation (λ = 1.54178 Å), employing a scanning rate of 0.02° s^{-1} in the 2θ range from 10 to 80°. The field emission scanning electron microscopy (FESEM) images were taken with a HITACHI S-4800 scanning electron microscope. Transmission electron microscopy (TEM) images and selected area electron diffraction (SAED) patterns were recorded on a JEOL JEM-2100 transmission electron microscope at an accelerating voltage of 200 kV. UV–vis absorption spectra and diffuse reflectance spectra (DRS) were recorded on a Lambda 950 UV/vis/NIR spectrophotometer (Perkin-Elmer, USA).

Methyl blue (MB) was used as a convenient photostable organic molecule to assay photochemical activity of p–n junction $Cu_2O/BiVO_4$ nanostructures. The prepared $Cu_2O/BiVO_4$ heterogeneous nanostructures (200 mg) were dispersed into an aqueous solution (100 mL) of methyl blue (10 mg L^{-1}). The suspension was sonicated for 5 min followed by stirring in dark for 30 min to ensure an adsorption-desorption equilibrium prior to irradiation. The suspension was then irradiated while stirring by using a 300-W Xe lamp (MAX-302, Asahi Spectra, USA) coupled with a UV cut off filter (λ > 420 nm). The initial and final reaction temperature for MB solution was measured at room temperature. Samples for analysis were taken from the reaction suspension after different reaction time and centrifuged at 6000 rpm for 5 min to remove the particles. The MB concentration from the upper clear solution was analyzed according to the absorption intensity at 664 nm in the measured UV–vis spectra.

The colorless organic phenol was further used to evaluate photocatalytic activity of the as-prepared $Cu_2O/BiVO_4$ heterogeneous nanostructures. In a typical experiment, 200 mg of $Cu_2O/BiVO_4$ heterogeneous nanostructures was added to 100 mL aqueous solution of phenol (100 mg L^{-1}). Before the photocatalytic degradation, the suspension was magnetically stirred in the dark for 30 min to establish a phenol adsorption/desorption equilibrium. Then the suspension was irradiated by using a 300-W Xe lamp (MAX-302, Asahi Spectra, USA) coupled with a UV cut off filter (λ > 420 nm) under stirring. Samples of 5 mL were collected from the suspension after different reaction time and were immediately centrifuged at 6000 rpm for 5 min. The concentration of phenol after illumination was determined spectrophotometrically at 270 nm using a Lambda 950 UV/vis/NIR spectrophotometer.

3. Results and discussion

Fig. 1 shows the XRD patterns of the as-prepared $BiVO_4$ nanocrystals and $Cu_2O/BiVO_4$ heterogeneous nanostructures with a quantity ratio of 1:2 of Cu_2O:$BiVO_4$. All diffraction peaks of pure $BiVO_4$ nanocrystals can be indexed based on a monoclinic $BiVO_4$ cell with lattice parameters of a = 5.195 Å, b = 11.701 Å, c = 5.092 Å and β = 90.38° (JCPDS No. 14-0668). The main peaks can be indexed as (0 2 0), (1 1 0), (0 1 1), (1 2 1), (0 4 0), (2 0 0), (0 0 2), (2 1 1), (1 1 2), (1 5 0), (1 3 2), (2 4 0), (0 4 2),(−2 0 2), (1 6 1), (2 5 1), (1 7 0), (3 2 1) and (1 2 3) planes of monoclinic $BiVO_4$. The XRD pattern of the as-prepared $Cu_2O/BiVO_4$ heterogeneous nanostructures is quite similar to that of the as-prepared pure $BiVO_4$ nanocrystals. No obvious peaks of Cu_2O can be detected. This is possibly due to the high crystallinity of the $BiVO_4$ phases, thus appearing as the dominant peaks in the XRD spectra of the $Cu_2O/BiVO_4$ heterogeneous nanostructures. However, a careful examination indicates that there is a weak peak at ca. 36.5°, which corresponds to the (1 1 1) plane of the Cu_2O as shown in enlarged XRD pattern (inset of Fig. 1).

The morphology and size of the as-prepared $BiVO_4$ nanocrystals and $Cu_2O/BiVO_4$ heterogeneous nanostructures were characterized by SEM. The SEM images reveal that that the as-prepared $BiVO_4$ nanocrystals exhibit plate-like morphology with thickness of about 100–400 nm, and some nanocrystals with irregular morphology as shown in Fig. 2a and b. Interestingly, one can seen that the surfaces of $BiVO_4$ nanocrystals are very smooth and clean as

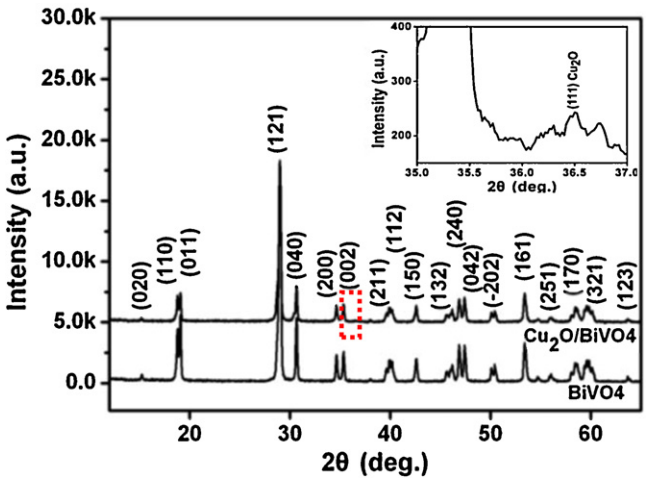

Fig. 1. XRD patterns of the pure $BiVO_4$ nanocrystals and $Cu_2O/BiVO_4$ heterogeneous nanostructure prepared with a quantity ratio of 1:2 of Cu_2O:$BiVO_4$.

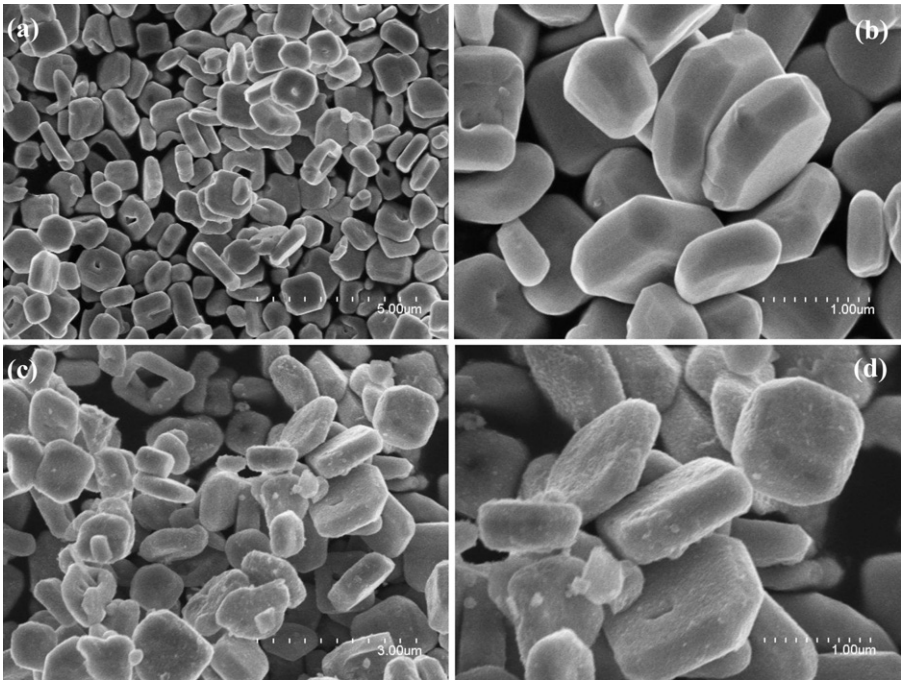

Fig. 2. SEM images of the as-prepared product: (a) and (b) pure $BiVO_4$ nanocrystals with different magnification, (c) and (d) $Cu_2O/BiVO_4$ heterogeneous nanostructures with different magnification.

presented in Fig. 2b. Fig. 2c and d shows the SEM images of the as-prepared $Cu_2O/BiVO_4$ heterogeneous nanostructures with different magnification. Fig. 2c is low magnification SEM images of the as-prepared $Cu_2O/BiVO_4$ heterogeneous nanostructures, indicating that a large number of Cu_2O nanoparticles are assembled on the surface of the $BiVO_4$ nanocrystals and all $BiVO_4$ nanocrystals have been covered by a layer of Cu_2O nanoparticles. Fig. 2d is higher magnification SEM images of the $Cu_2O/BiVO_4$ heterogeneous nanostructures, which shows that the size of Cu_2O nanoparticles on the surface of the $BiVO_4$ nanocrystals is uniform. Meanwhile, higher magnification SEM images of the as-prepared $Cu_2O/BiVO_4$ heterogeneous nanostructures clearly demonstrate a higher distribution density of Cu_2O nanoparticles on the surface of the $BiVO_4$ nanocrystals.

Fig. 3 shows the TEM images of the as-prepared $BiVO_4$ nanocrystals and $Cu_2O/BiVO_4$ heterogeneous nanostructures with a quantity ratio of 1:2 of Cu_2O:$BiVO_4$. The TEM image in Fig. 3a shows that the $BiVO_4$ nanocrystals are composed of crystals with plate-like and irregular morphology. Interestingly, we found that a few crystals have a hollow interior structure as shown in a typical TEM image of an individual square-like crystal (Fig. 3b). Fig. 3c–f shows the TEM images of the as-prepared $Cu_2O/BiVO_4$ heterogeneous nanostructures with different magnification. Fig. 3c is low magnification TEM image of the $Cu_2O/BiVO_4$ heterogeneous nanostructures, showing that a large number of Cu_2O nanoparticles are assembled on the all surfaces of the $BiVO_4$ nanocrystals. Higher magnification TEM image as presented in Fig. 3d shows that the size of the Cu_2O nanoparticles is uniform. Fig. 3e is a typical TEM image of an individual $Cu_2O/BiVO_4$ heterogeneous nanostructure with hollow interior structure. Again, one can see Cu_2O nanoparticles assemble on the surface of the $BiVO_4$ nanocrystals with high distribution density. High magnifications TEM image as shown in Fig. 3f shows that the size of the Cu_2O nanoparticles is in the range of 5–20 nm.

Fig. 4a is a typical TEM image of an individual square-like $Cu_2O/BiVO_4$ heterogeneous nanostructure that is further used to investigate the microstructure features. Fig. 4b is the HRTEM image of the individual square-like $Cu_2O/BiVO_4$ heterogeneous nanostructure as presented in Fig. 4a. The HRTEM image clearly confirms that the Cu_2O nanoparticles are tiny nanocrystals uniformly distributed on the surface of the $BiVO_4$ nanocrystals and contact with $BiVO_4$ nanocrystals tightly, resulting in a heterogeneous nanostructure on the surface of the $BiVO_4$ nanocrystals. As shown in Fig. 4b, on the surface of $Cu_2O/BiVO_4$ heterogeneous nanostructure, there are two different crystal structures with the interplanar spacing of ca 0.262 nm and 0.242 nm, which correspond to the (2 0 0) planes of monoclinic $BiVO_4$ and (1 1 1) planes of cubic Cu_2O, respectively. Fig. 4c is a typical TEM image of an individual $Cu_2O/BiVO_4$ heterogeneous nanostructure with hollow interior. The HRTEM image of this nanostructure is presented in Fig. 4e. Again, one can clearly see that the Cu_2O nanoparticles are attached to the surface of $BiVO_4$ nanocrystals. The corresponding interplanar spacing is ca 0.260 nm and 0.241 nm, which also correspond to the (2 0 0) planes of monoclinic $BiVO_4$ and (1 1 1) planes of cubic Cu_2O, respectively. The HRTEM images show that the Cu_2O nanoparticles are intimately attached to the surface of $BiVO_4$ nanocrystals, and hence a well-defined heterostructure is generated. Because Cu_2O and $BiVO_4$ are p-type and n-type semiconductors, respectively, the heterojunction can be considered to be a well-defined and well-formed nano-p–n junction. One also can find that most of the Cu_2O nanoparticles are well developed polyhedrons with different orientations due to the orientational difference of the nuclei that are initially formed on the surface of $BiVO_4$ nanocrystals.

The composition and microstructure features of the Cu_2O nanoparticles were further studied by SAED and HRTEM. The nanoparticles attached to the surface of an individual $Cu_2O/BiVO_4$ heterogeneous nanostructure as shown in Fig. 5a were used to make further SAED and HRTEM characterizations. Fig. 5b is SAED pattern taken from the attached nanoparticles in $Cu_2O/BiVO_4$ heterogeneous nanostructure of Fig. 5a. The ring pattern reseals the polycrystalline nature of the formed nanoparticles. The diffraction rings of the SAED pattern can be indexed on a cubic cell of Cu_2O with lattice parameter of $a = 4.269$ Å, showing that the nanoparticles in $Cu_2O/BiVO_4$ heterogeneous nanostructure consist of only cubic Cu_2O. The HRTEM image of the nanoparticles is presented in

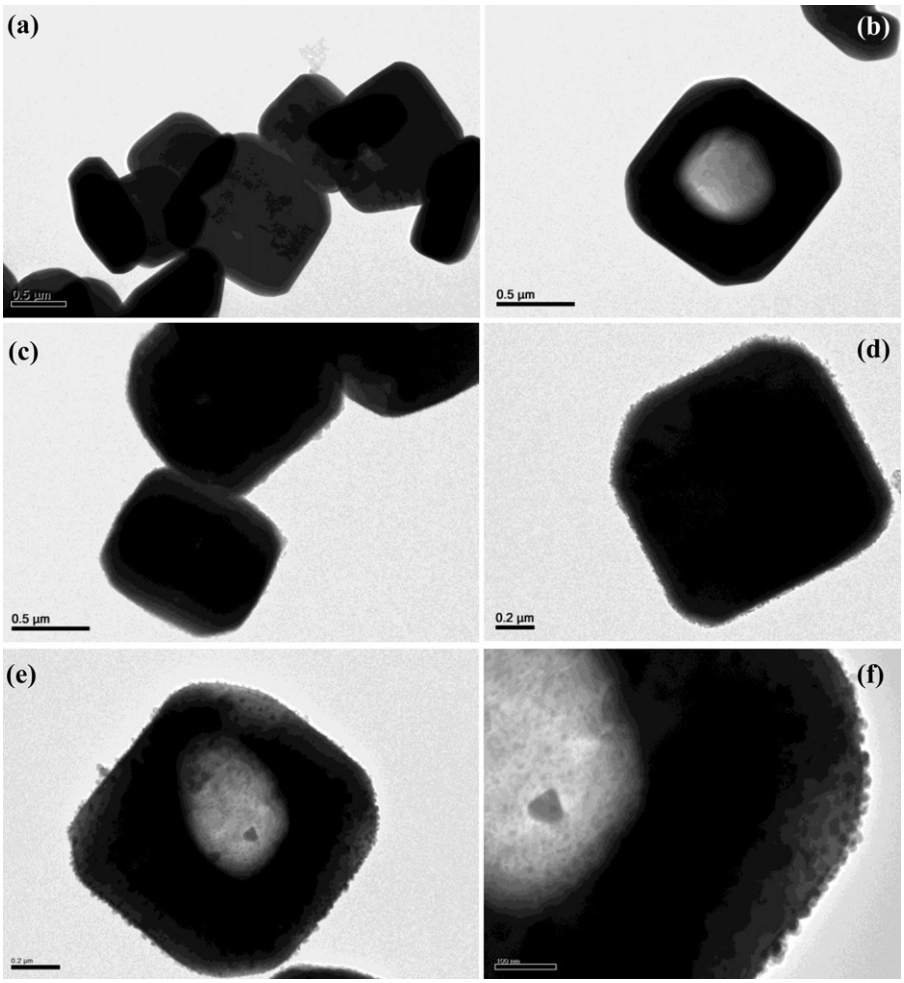

Fig. 3. (a) TEM images of the as-prepared pure $BiVO_4$ nanocrystals. (b) TEM image of an individual $BiVO_4$ nanocrystal with hollow interior structure. (c) TEM images of the as-synthesized $Cu_2O/BiVO_4$ heterogeneous nanostructures. (d) TEM image of an individual $Cu_2O/BiVO_4$ heterogeneous nanostructure, clearly showing that a large number of Cu_2O nanoparticles are assembled on the all surfaces of the $BiVO_4$ nanocrystal. (e) TEM image of an individual $Cu_2O/BiVO_4$ heterogeneous nanostructure with hollow interior structure. (f) An enlarged TEM image of an individual $Cu_2O/BiVO_4$ heterogeneous nanostructure in (e), showing that Cu_2O nanoparticles assemble on the surface of the $BiVO_4$ nanocrystal with high distribution density.

Fig. 5c, showing that the nanoparticles are randomly attached to the surface of $BiVO_4$ nanocrystals with different growth direction. The enlarged HRTEM image as presented in Fig. 5d demonstrates that the nanoparticles are crystallized with the interplanar spacing of about 0.246 nm, which is corresponding to the (1 1 1) planes of cubic Cu_2O. Thus, the SAED and HRTEM further verify that the nanoparticles attached to the surface of the $BiVO_4$ nancrystals are composed of pure cubic Cu_2O.

The diffuse reflectance spectra of the prepared $BiVO_4$ and $Cu_2O/BiVO_4$ samples with a quantity ratio of 1:2 of Cu_2O:$BiVO_4$ are shown in Fig. 6a. The value of the band gap energies of the as-prepared $BiVO_4$ and $Cu_2O/BiVO_4$ can be evaluated by the equation $\alpha E_{photon} = K(E_{photon} - E_g)^{1/2}$, where α is the absorption coefficient, E_{photon} is the discrete photo energy, K is a constant and E_g is the band gap energy. A classical Tauc approach is further used to estimate the E_g values of the as-prepared $BiVO_4$ and $Cu_2O/BiVO_4$. The plot of $(\alpha E_{photon})^2$ vs E_{photon} based on the direct transition is presented in Fig. 6b. The extrapolated value (the straight line to the χ axis) of E_{photon} at $\alpha = 0$ gives absorption edge energies of 2.48 and 2.45 eV for $BiVO_4$ and $Cu_2O/BiVO_4$, respectively.

The photocatalytic activities of the prepared $BiVO_4$ nanocrystals and $Cu_2O/BiVO_4$ heterogeneous nanostructures were evaluated through MB degradation under visible-light ($\lambda > 420$ nm) irradiation. Fig. 7a and b shows the temporal absorption spectral changes of MB in photo-degradation over the as-prepared $BiVO_4$ nanocrystals and $Cu_2O/BiVO_4$ heterogeneous nanostructures catalysts under visible-light irradiation. The result indicated that an obvious absorption peak at 664 nm can be observed with the as-prepared $BiVO_4$ nanocrystals as catalyst after irradiation for 4 h (Fig. 7a). However, when the as-synthesized $Cu_2O/BiVO_4$ heterogamous nanostructures were used as catalyst, the absorption band at 664 nm was almost disappeared as shown in Fig. 7b, showing the prepared $Cu_2O/BiVO_4$ heterogamous nanostructures have enhanced photocatalytic activity compared to the prepared pure $BiVO_4$ nanocrystals. Fig. 7c shows the photocatalytic degradation rates (C/C_0) of the MB on the $BiVO_4$ nanocrystals and $Cu_2O/BiVO_4$ heterogeneous nanostructures, where C_0 is the initial concentration of MB, C is the concentration of MB at different irradiation time. The results indicated that about 97.3% of MB was degraded by using $Cu_2O/BiVO_4$ heterogeneous nanostructures as catalyst after irradiating 4 h with visible-light. However, about 78.2% of MB was degraded by using the prepared pure $BiVO_4$ nanocrystals as catalyst at the constant experimental conditions. The results show that the photocatalytic activity of the $Cu_2O/BiVO_4$ heterogeneous nanostructures on degradation of MB is significantly enhanced compared to the prepared pure $BiVO_4$ nanocrystals.

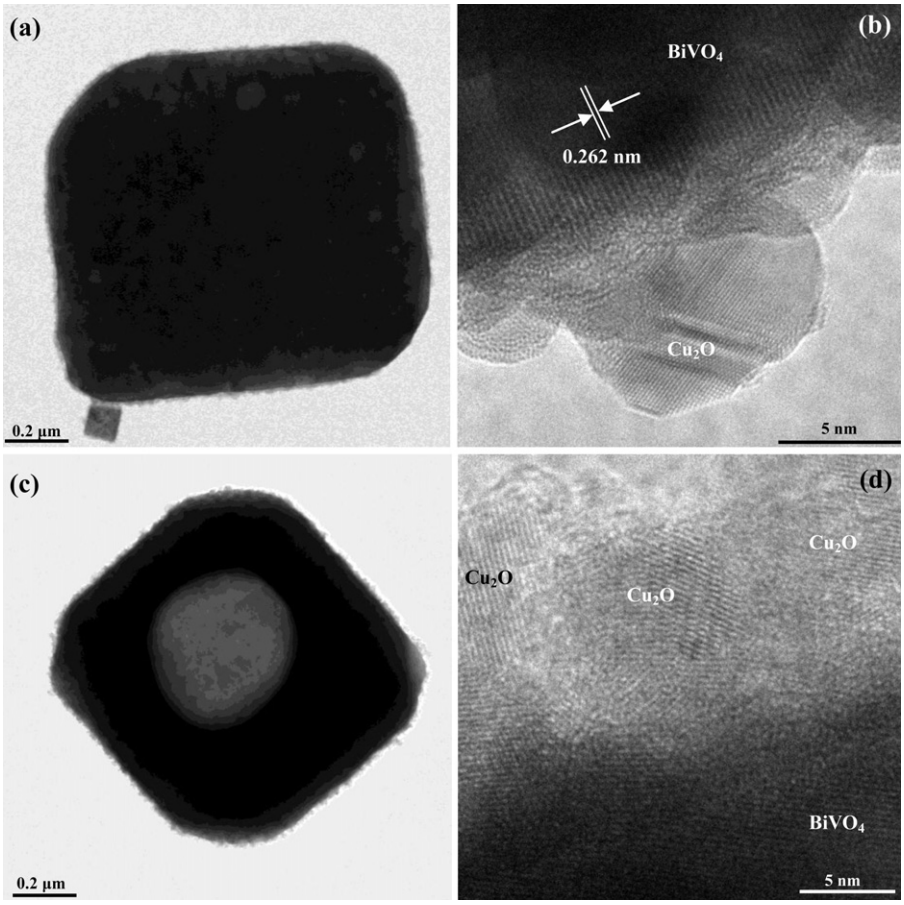

Fig. 4. (a) TEM image of an individual $Cu_2O/BiVO_4$ heterogeneous nanostructure used to make further microstructure investigation. (b) HRTEM image of an individual $Cu_2O/BiVO_4$ heterogeneous nanostructure in (a). (c) TEM image of an individual $Cu_2O/BiVO_4$ heterogeneous nanostructure with hollow interior structure used to make further microstructure investigation and (d) corresponding HRTEM image of (c).

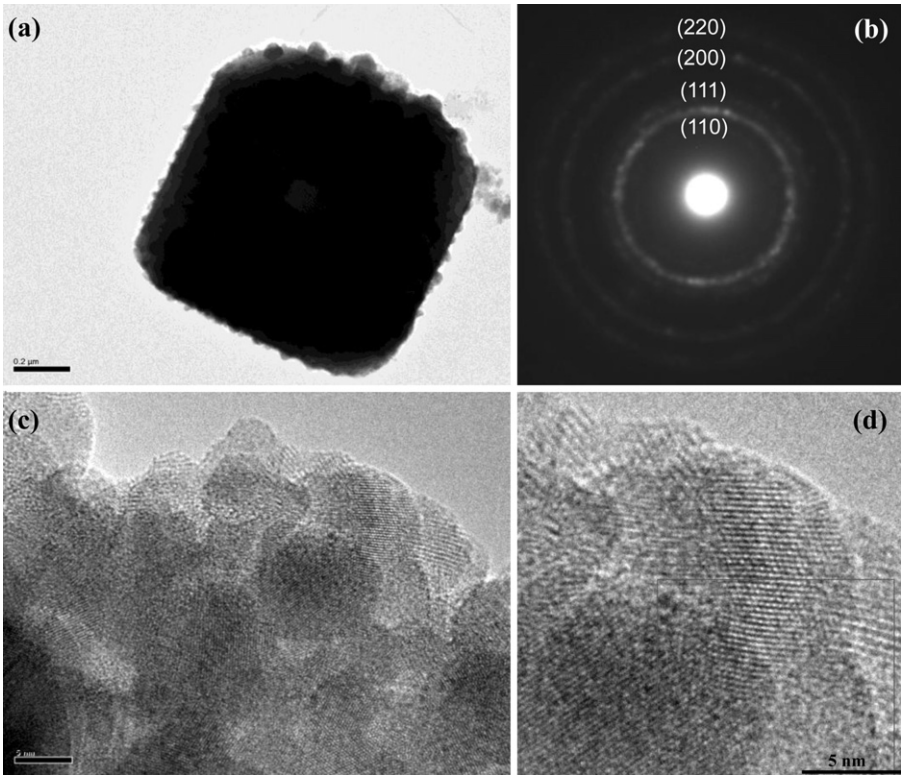

Fig. 5. (a) TEM image of the nanoparticles attached to the surface of an individual $BiVO_4$ nanostructure. (b) SAED pattern taken from the attached nanoparticles in $Cu_2O/BiVO_4$ heterogeneous nanostructure of (a). (c) HRTEM image of the nanoparticles as shown in (a).

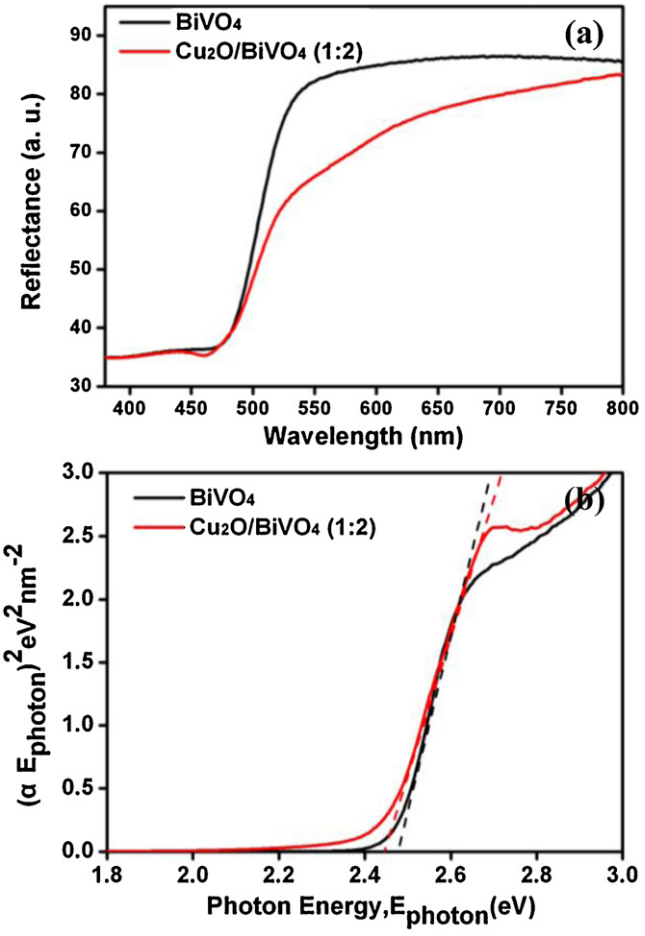

Fig. 6. (a) Diffuse reflectance spectra of $BiVO_4$ and $Cu_2O/BiVO_4$ structures. (b) Band gap energy of the as-prepared pure $BiVO_4$ crystals and $Cu_2O/BiVO_4$ heterogeneous nanostructures.

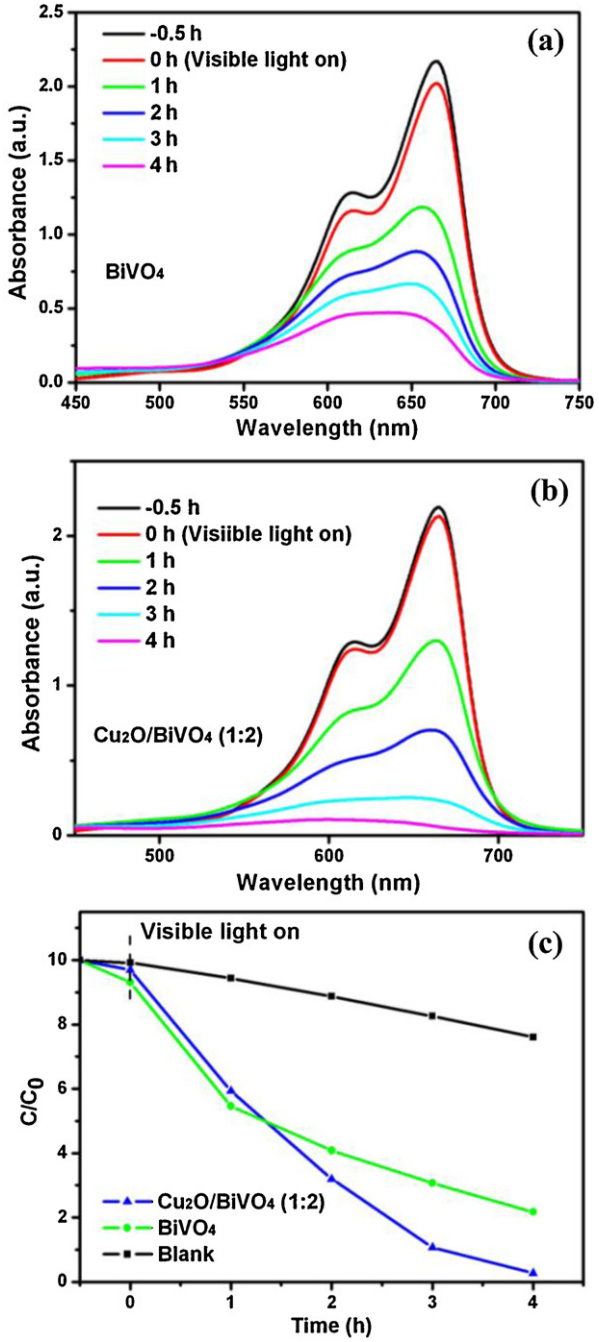

Fig. 7. (a) Time-dependent UV–vis absorption spectra of the MB solution in the presence of various photocatalysts: (a) pure BiVO4, (b) $Cu_2O/BiVO_4$ heterogeneous nanostructures. (c) photocatalytic degradation ratio of MB versus visible light ($\lambda > 420$ nm) irradiation time by using various photocatalysts.

The influence of the Cu precursor amount to the Cu_2O morphology and the photocatalytic activity also has been investigated. Fig. 8 shows the SEM images of $Cu_2O/BiVO_4$ heterogeneous nanostructures prepared with different Cu precursor amount. With a quantity ratio of 1:3 of Cu_2O:$BiVO_4$, SEM images indicate that the $BiVO_4$ nanocrystals have been covered by a layer of Cu_2O nanoparticles as shown in Fig. 8a and b. However, it can be seen from SEM a high magnification SEM image (Fig. 8b) that density of Cu_2O nanoparticles on the surface of the $BiVO_4$ nanocrystals is lower than that of $Cu_2O/BiVO_4$ heterogeneous nanostructures with a quantity ratio of 1:2 of Cu_2O:$BiVO_4$ (Fig. 2d). With increase the amount of Cu precursor to make a quantity ratio of 1:1 of Cu_2O:$BiVO_4$, one also can find that the $BiVO_4$ nanocrystals were covered by a layer of Cu_2O nanoparticles as shown in Fig. 8c. However, one also can find that some excess Cu_2O nanoparticles gather to form aggregate on the surface of $BiVO_4$ nanocrystals as clearly shown in Fig. 8d. Meanwhile, SEM image also indicates that some excess Cu_2O nanoparticles assemble to form nanostructure with cubic morphology.

The influence of the Cu precursor amount to the photocatalytic activities of $Cu_2O/BiVO_4$ heterogeneous nanostructures has been investigated through MB degradation under visible-light ($\lambda > 420$ nm) irradiation. The temporal absorption spectral changes of MB in photo-degradation over the $Cu_2O/BiVO_4$ heterogeneous nanostructures catalysts with different Cu precursor amount were shown in Fig. 9a and b. Fig. 9a shows the temporal absorption spectral changes of MB in photo-degradation over the $Cu_2O/BiVO_4$ heterogeneous nanostructures catalyst with a quantity ratio of 1:1 of Cu_2O:$BiVO_4$. One can find that an obvious absorption peak at 664 nm can be observed. However, when the $Cu_2O/BiVO_4$ heterogamous nanostructures with a quantity ratio of 1:3 of Cu_2O:$BiVO_4$ were used as catalyst, the absorption band at 664 nm was almost disappeared as presented in Fig. 9b. Fig. 9c shows the photocatalytic degradation rates (C/C_0) of the MB on the $Cu_2O/BiVO_4$ heterogeneous nanostructures with different Cu_2O:$BiVO_4$ quantity ratio, where C_0 is the initial concentration of MB, C is the concentration of MB at different irradiation time. When the $Cu_2O/BiVO_4$ heterogeneous

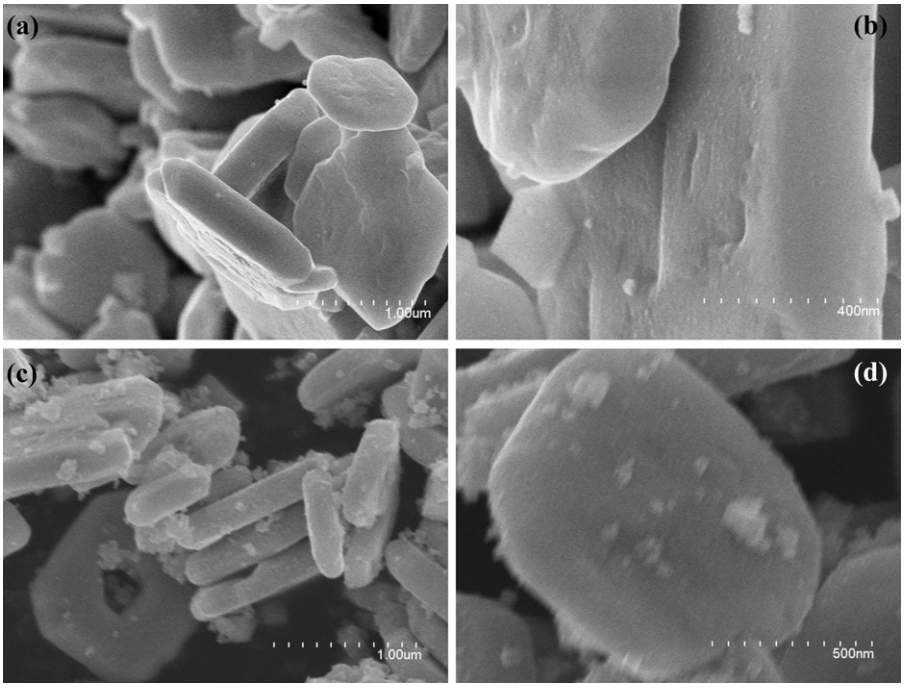

Fig. 8. (a) and (b) Low- and high-magnification SEM images the as-prepared $Cu_2O/BiVO_4$ heterogeneous nanostructures with a quantity ratio of 1:3 of Cu_2O:$BiVO_4$. (c) and (d) Low- and high-magnification SEM images the as-prepared $Cu_2O/BiVO_4$ heterogeneous nanostructures with a quantity ratio of 1:1 of Cu_2O:$BiVO_4$.

nanostructures with a quantity ratio of 1:3 of Cu_2O:$BiVO_4$ were used as catalyst, one can see that about 95.7% of MB was degraded after irradiating 4 h with visible-light. However, about 69.8% of MB was degraded by using the $Cu_2O/BiVO_4$ heterogeneous nanostructures with a quantity ratio of 1:1 of Cu_2O:$BiVO_4$ as catalyst at the constant experimental conditions. The results indicate that the amount of Cu_2O in $Cu_2O/BiVO_4$ heterogeneous nanostructures can significantly influence on the photocatalytic activity of the heterogeneous nanostructures on the degradation of MB. From Fig. 9c, one can find that the MB conversion over the as-fabricated catalysts within 4 h of reaction decreased in the order of $Cu_2O/BiVO_4$ (ca. 97.3%; Cu_2O:$BiVO_4$ of 1:2) > $Cu_2O/BiVO_4$ (ca. 95.7%; Cu_2O:$BiVO_4$ of 1:3) > $BiVO_4$ (ca. 78.3; pure $BiVO_4$) > $Cu_2O/BiVO_4$ (ca. 69.8%; Cu_2O:$BiVO_4$ of 1:1). The above results indicate that an insufficient Cu_2O amount in $Cu_2O/BiVO_4$ heterogeneous nanostructures cannot effectively separate electrons and holes photogenerated from nanostructures, resulting in a low photocatalytic activity. On the other hand, an excess Cu_2O amount in heterogeneous nanostructures can also decrease the photocatalytic activity of the nanostructures as shown in $Cu_2O/BiVO_4$ heterogeneous nanostructures with a quantity ratio of 1:1 of Cu_2O: $BiVO_4$, because excess Cu_2O can offer as the recombination centers of electron–hole pairs, leading to a less photocatalytic activity.

The photocatalytic activities of the prepared pure $BiVO_4$ nanocrystals and $Cu_2O/BiVO_4$ heterogeneous nanostructures were further evaluated for the degradation of phenol, which is a colorless organic, under visible-light ($\lambda > 420$ nm) irradiation. Fig. 10a and b shows the temporal absorption spectral changes of phenol in photo-degradation over the as-prepared pure $BiVO_4$ nanocrystals and $Cu_2O/BiVO_4$ heterogeneous nanostructures catalysts with a quantity ratio of 1:2 of Cu_2O: $BiVO_4$. Although an obvious absorption peak at 270 nm can be observed with the pure $BiVO_4$ nanocrystals and $Cu_2O/BiVO_4$ heterogeneous nanostructures as catalysts after irradiation for 4 h, the absorption band at 270 nm was much reduced with $Cu_2O/BiVO_4$ heterogeneous nanostructures as catalyst as shown in Fig. 10b, compared to the pure $BiVO_4$ nanocrystals catalyst (Fig. 10a). Fig. 10c shows the photocatalytic degradation rates (C/C_0) of the phenol on the pure $BiVO_4$ nanocrystals and $Cu_2O/BiVO_4$ heterogeneous nanostructures, where C_0 is the initial concentration ofphenol, C is the concentration of phenol at different irradiation time. The results indicated that about 41.0% of phenol was degraded by using $Cu_2O/BiVO_4$ heterogeneous nanostructures as catalyst. However, about 20.0% of phenol was degraded by using the prepared pure $BiVO_4$ nanocrystals as catalyst at the constant experimental conditions. The photocatalytic degradation rates (C/C_0) of the phenol for $Cu_2O/BiVO_4$ heterogeneous nanostructures (41.0%) is more than two times higher than that of pure $BiVO_4$ nanocrystals. This further confirms the high visible-light photocatalytic efficiency of the $Cu_2O/BiVO_4$ heterogeneous nanostructures.

The enhanced photocatalytic activity of the $Cu_2O/BiVO_4$ heterogeneous nanostructures compared to the pure $BiVO_4$ nanocrystals can be ascribed to formation of the p–n junction between p-type Cu_2O and n-type $BiVO_4$ semiconductors. It has been reported that the conduction band (CB) and valence band (VB) potentials of the p-type Cu_2O semiconductor are 1.4 eV and 0.6 eV, respectively. The CB and VB potentials of the n-type $BiVO_4$ semiconductor are 0.28 eV and 2.78 eV, respectively. Fig. 11a shows the energy-band schematic diagram for p-type Cu_2O and n-type $BiVO_4$. Thus, before contact of p-type Cu_2O semiconductor and n-type $BiVO_4$ semiconductor, the conduction band edge of p-type Cu_2O is higher than that of n-type $BiVO_4$, and the Fermi level of the Cu_2O is lower than that of the $BiVO_4$. After contact of Cu_2O and $BiVO_4$, the Fermi level of Cu_2O is moved up; while the Fermi level of $BiVO_4$ is moved down until an equilibrium state is formed as shown in Fig. 11b. Meanwhile, consistent with the rising up and/or descending of the Fermi level, the whole energy band of Cu_2O is raised up while that of $BiVO_4$ is descended, and as a result, the conduction band edge of Cu_2O is much higher than that of $BiVO_4$. Thus at the equilibrium, an inner electric field from n-type $BiVO_4$ to p-type Cu_2O is established. Under visible-light irradiation, both Cu_2O and $BiVO_4$ can be excited to generate electron–hole pairs. According to the energy-band schematic diagram in Fig. 11, the photogenerated electrons

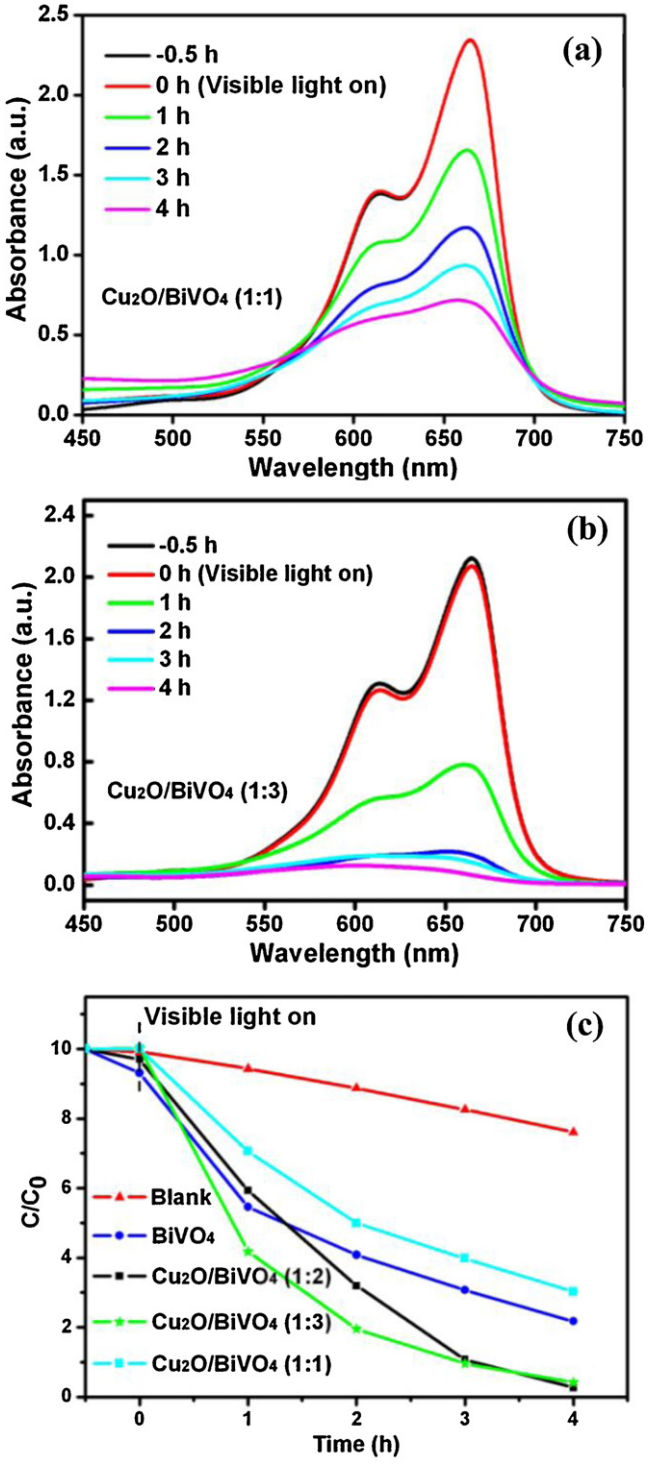

Fig. 9. (a) Time-dependent UV-vis absorption spectra of the MB solution in the presence of various photocatalysts: (a) $Cu_2O/BiVO_4$ heterogeneous nanostructures with a quantity ratio of 1:1 of Cu_2O:$BiVO_4$. (b) $Cu_2O/BiVO_4$ heterogeneous nanostructures with a quantity ratio of 1:3 of Cu_2O:$BiVO_4$. (c) photocatalytic degradation ratio of MB versus visible light ($\lambda > 420$ nm) irradiation time by using various photocatalysts.

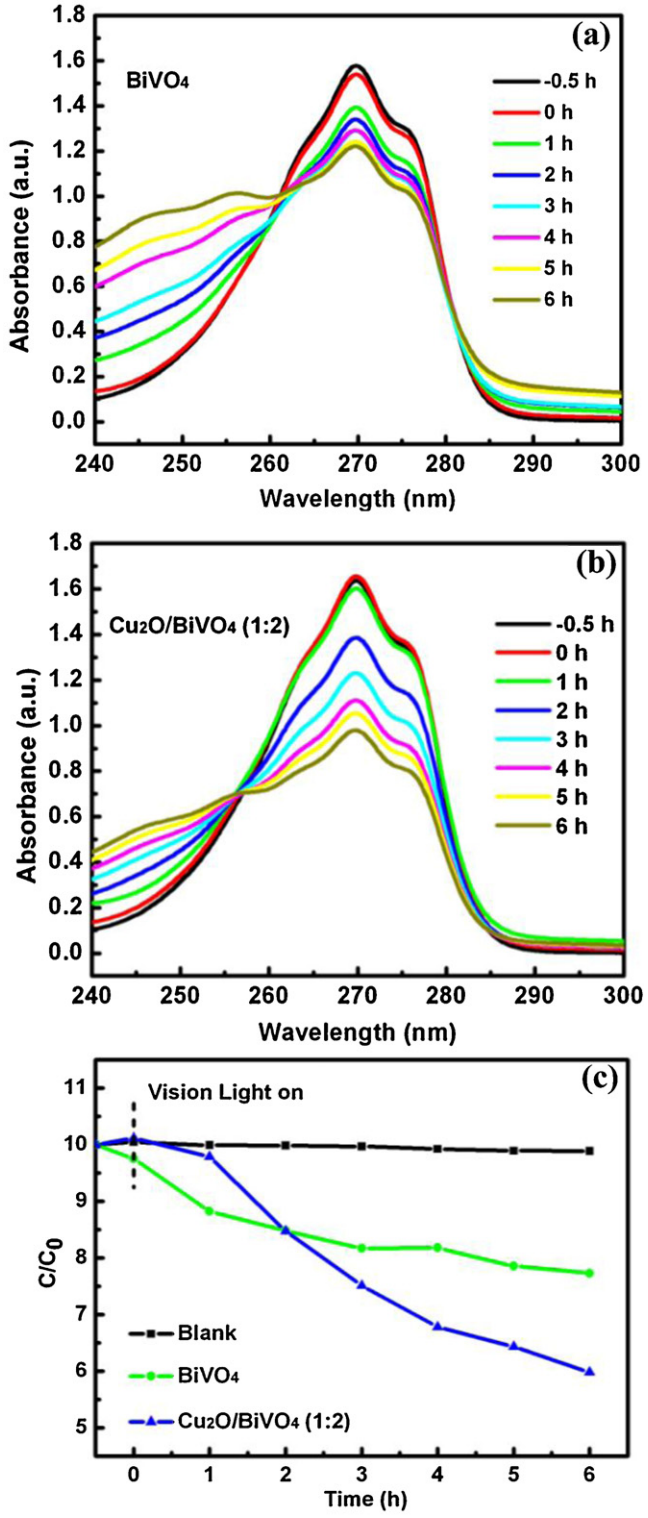

Fig. 10. (a) Time-dependent UV–vis absorption spectra of the phenol solution in the presence of various photocatalysts: (a) pure BiVO4, (b) $Cu_2O/BiVO_4$ heterogeneous nanostructures with a quantity ratio of 1:2 of Cu_2O:$BiVO_4$. (c) Photocatalytic degradation ratio of MB versus visible light ($\lambda > 420$ nm) irradiation time by using various photocatalysts.

on the conduction band of the p-type Cu_2O can transfer to that of n-type $BiVO_4$, and holes remain in the p-Cu_2O valence band, while simultaneously photogenerated holes can migrate from the valence band of n-type $BiVO_4$ to that of p-type Cu_2O. The migration of photogenerated carriers can be promoted by the internally formed electric field. Therefore, the photogenerated electrons and holes can be separated effectively by the p–n junction formed between the p-type Cu_2O and n-type $BiVO_4$ interface, and the recombination of electron-hole pairs can be substantially reduced. Thus the separated electrons and holes are then free to initiate reactions with the reactants adsorbed on the photocatalyst surface, leading to an enhanced photocatalytic activity.

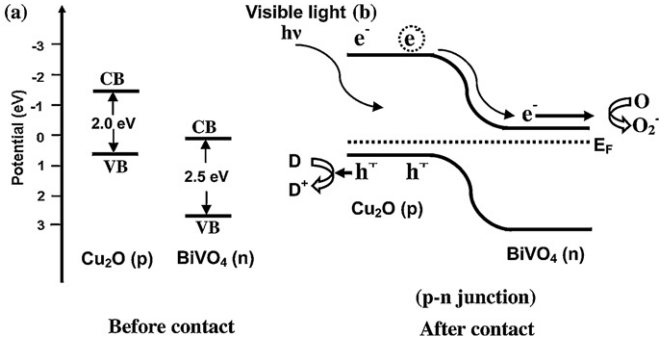

Fig. 11. Schematic diagram of charge transfer between p-type Cu_2O and n-type$BiVO_4$: (a) before contact; (b) after formation of the p–n junction.

4. Conclusions

p–n junction $Cu_2O/BiVO_4$ heterogeneous nanostructures for enhancement of visible-light photocatalytic properties of $BiVO_4$ nanocrystals have been successfully prepared through coupling a hydrothermal process with polyol strategy. HRTEM investigations indicated that a large number of nano p–n junction heterostructures on the surface of the $BiVO_4$ nanocrystals were formed by the assembly of p-type Cu_2O nanoparticles, where Cu_2O and $BiVO_4$ form p- and n-type semiconductors, respectively. The photocatalytic activity tests demonstrate that these p–n junction $Cu_2O/BiVO_4$ heterogeneous nanostructures exhibit highly efficient visible-light-driven photocatalytic activities as compared to the individual $BiVO_4$ nanocrystals for the degradation of model dyes methylene blue and colorless organic phenol under visible light irradiation. The improved photocatalytic efficiencies are attributed to the enhanced charge separation by the contacting Cu_2O nanoparticles, allowing the photogenerated electrons and holes to have sufficient time to participate the overall photocatalytic reactions. We believe that our strategy of the heterostructure synthesis involving tethered p-type Cu_2O semiconductor nanoparticles on a n-type semiconductor surface for enhancing photocatalytic activities can have considerable impact on the future development of highly efficient visible-light p–n junction photocatalysts for organic pollutant degradation.

Acknowledgements

This work was supported by National Natural Science Foundation of China (NSFC, Grants No. 11074312), Undergraduate Innovative Test Program of China (GCCX2012110011), “985 project” (Nos. 98507-010009) and “211 project” of Ministry of Education of China and the Fundamental Research Funds for the Central Universities (No. 0910KYZD04).

References

[1] A. Iwase, A. Kudo, Journal of Materials Chemistry 20 (2010) 7536–7542.
[2] D.G. Wang, H.F. Jiang, X. Zong, Q. Xu, Y. Ma, G.L. Li, C. Li, Chemistry: A European Journal 17 (2011) 1275–1282.
[3] T. Saison, N. Chemin, C. Chaneĭac, O. Durupthy, V. Ruaux, L. Mariey, F. Maugeĭ, P. Beaunier, J.-P. Jolivet, Journal of Physical Chemistry C 115 (2011) 5657–5666.
[4] L.S. Zhang, W.Z. Wang, J. Yang, Z.G. Chen, W.Q. Zhang, L. Zhou, S.W. Liu, Applied Catalysis A: General 308 (2006) 105–110.
[5] D. Chen, J.H. Ye, Advanced Functional Materials 18 (2008) 1922–1928.
[6] T. Arai, M. Yanagida, Y. Konishi, A. Ikura, Y. Iwasaki, H. Sugihara, K. Sayama, Applied Catalysis B 84 (2008) 42–47.
[7] A. Duret, M. Grätzel, Journal of Physical Chemistry B 109 (2005) 17184–17191.
[8] H. Xie, Y.Z. Li, S.F. Jin, J.J. Han, X.J. Zhao, Journal of Physical Chemistry C 114 (2010) 9706–9712.
[9] C.H. Kuo, C.H. Chen, M.H. Huang, Advanced Functional Materials 17 (2007) 3773–3780.
[10] S. Somasundaram, C. Ramannairchenthamarakshan, N. Detacconi, K. Rajeshwar, International Journal of Hydrogen Energy 32 (2007) 4661–4669.
[11] P. Chatchai, Y. Murakami, S. -Y, A.Y. Kishioka, Y. Nosaka, Nosaka, Electrochimica Acta 54 (2009) 1147–1152.
[12] H.-Q. Jiang, H. Endo, H. Natori, M. Nagai, K. Kobayashi, Materials Research Bulletin 44 (2009) 700–706.
[13] A. Kudo, K. Omori, H. Kato, Journal of the American Chemical Society 121 (1999) 11459–11467.
[14] S. Tokunaga, H. Kato, A. Kudo, Chemistry of Materials 13 (2001) 4624–4628.
[15] S. Kohtania, M. Koshiko, A. Kudo, K. Tokumura, Y. Ishigaki, A. Toriba, K. Hayakawa, R. Nakagaki, Applied Catalysis B 46 (2003) 573–586.
[16] S. Kohtani, J. Hiro, N. Yamamoto, A. Kudo, K. Tokumura, R. Nakagaki, Catalysis Communication 6 (2005) 185–189.
[17] J. Yu, A. Kudo, Advanced Functional Materials 16 (2006) 2163–2169.
[18] X. Zhang, Z. Ai, F. Jia, L. Zhang, X. Fan, Z. Zou, Materials Chemistry and Physics 103 (2007) 162–167.
[19] L. Ge, Materials Chemistry and Physics 107 (2008) 465–470.
[20] J. Yu, Y. Zhang, A. Kudo, Journal of Solid State Chemistry 182 (2009) 223–228.
[21] Y. Zhou, K. Vuille, A. Heel, B. Probst, R. Kontic, G. Patzke, Applied Catalysis A: General 375 (2010) 140–184.
[22] G.C. Xi, J.H. Ye, Chemical Communication 46 (2010) 1893–1895.
[23] Y.B. Wan, S.H. Wang, W.H. Luo, L.H. Zhao, International Journal of Photoenergy (2012) 7.
[24] P. Chatchai, S.-Y. Kishioka, Y. Murakami, A.Y. Nosaka, Y. Nosaka, Electrochimica Acta 55 (2010) 592–596.
[25] S. Hu, F. Zhou, L. Wang, J. Zhang, Catalysis Communication 12 (2011) 794–797.
[26] L. Li, B. Yan, Journal of Non-Crystalline Solids 355 (2009) 776–779.
[27] R. Liu, H. Ye, X. Xiong, H. Liu, Materials Chemistry and Physics 121 (2010) 432–439.
[28] M. Agrawal, S. Gupta, A. Pich, N.E. Zafeiropoulos, M. Stamm, Chemistry of Materials 21 (2009) 5343–5348.
[29] K. Lv, J. Li, X.X. Qing, W.Z. Li, Q.Y. Chen, Journal of Hazardous Materials 189 (2011) 329–335.
[30] N. Wetchakun, S. Chaiwichain, B. Inceesungvorn, K. Pingmuang, S. Phanichphant, A.I. Minett, J. Chen, ACS Applied Materials and Interfaces 4 (2012) 3718–3723.
[31] M. Shang, W.Z. Wang, L. Zhang, S.M. Sun, L. Wang, L. Zhou, Journal of Physical Chemistry C 113 (2009) 14727–14731.
[32] B. Nikoobakht, J. Bonevich, A. Herzing, Journal of Physical Chemistry C 115 (2011) 9961–9969.
[33] X.N. Li, R.K. Huang, Y.H. Hu, Y.J. Chen, W.J. Liu, R.S. Yuan, Z.H. Li, Inorganic Chemistry 51 (2012) 6245–6250.
[34] P. He, X. Shen, H. Gao, Journal of Colloids and Interface Science 284 (2005) 510–515.
[35] L. Li, M. Zhang, Journal of Optoelectronics and Advanced Materials 13 (2011) 719–721.